

Élivágar: Efficient Quantum Circuit Search for Classification

Sashwat Anagolum*
Pennsylvania State University

Narges Alavisamani
Georgia Institute of Technology

Poulami Das
University of Texas, Austin

Moinuddin Qureshi
Georgia Institute of Technology

Eric Kessler
AWS Quantum Technologies

Yunong Shi
AWS Quantum Technologies

Abstract

Designing performant and noise-robust circuits for Quantum Machine Learning (QML) is challenging — the design space scales exponentially with circuit size, and there are few well-supported guiding principles for QML circuit design. Although recent Quantum Circuit Search (QCS) methods attempt to search for performant QML circuits that are also robust to hardware noise, they directly adopt designs from classical Neural Architecture Search (NAS) that are misaligned with the unique constraints of quantum hardware, resulting in high search overheads and severe performance bottlenecks.

We present *Élivágar*, a novel resource-efficient, noise-guided QCS framework. *Élivágar* innovates in all three major aspects of QCS — search space, search algorithm and candidate evaluation strategy — to address the design flaws in current classically-inspired QCS methods. *Élivágar* achieves hardware-efficiency and avoids an expensive circuit-mapping co-search via noise- and device topology-aware candidate generation. By introducing two cheap-to-compute predictors, Clifford noise resilience and representational capacity, *Élivágar* decouples the evaluation of noise robustness and performance, enabling early rejection of low-fidelity circuits and reducing circuit evaluation costs. Due to its resource-efficiency, *Élivágar* can further search for data embeddings, significantly improving performance.

Based on a comprehensive evaluation of *Élivágar* on 12 real quantum devices and 9 QML applications, *Élivágar* achieves 5.3% higher accuracy and a $271\times$ speedup compared to state-of-the-art QCS methods.

1. Introduction

Quantum Machine Learning (QML) is an important class of quantum algorithms for the *Noisy-Intermediate Scale Quantum (NISQ)* [65] era, due to its applicability to real-world problems such as classification [20, 28, 42, 80], generative modeling [26, 54, 70, 96, 97] and learning physical systems [27, 41]. QML uses *variational* quantum circuits to perform machine learning tasks. The parameters in these variational circuits are iteratively updated (i.e., *trained*) using a classical optimizer until the circuit learns the input problem to high accuracy.

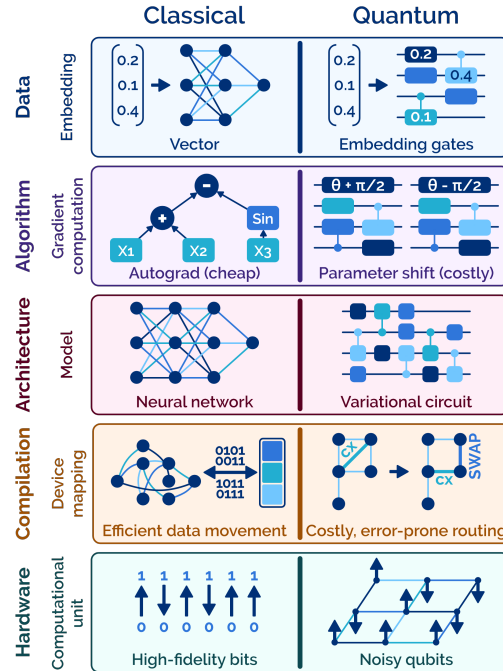


Figure 1: Comparison of classical and quantum ML systems.

The key challenge in designing effective near-term QML algorithms is to find variational circuits with good *circuit performance*, to accurately learn the input problem, and *noise robustness*, to avoid performance degradation. However, due to the complexity of device-level noise sources and the nascent state of QML theory, there are few established guiding principles in designing QML circuits. Current manually crafted circuits are often under-performant, and face numerous practical issues such as vanishing gradients [84] and low fidelity.

This challenge has motivated recent efforts in **Quantum Circuit Search (QCS)** [18, 80, 94] which aims to automatically find high-performance, noise-robust circuits. While promising, these methods are still preliminary, and naively adopt established methodologies from classical Neural Architecture Search (NAS) [36, 53], a subfield of Machine Learning (ML) that searches for high-performance neural networks. As a result, current QCS works overlook the fundamental differences between classical ML and QML, shown in Fig. 1.

At the data processing level, classical ML uses multi-dimensional vectors to represent input data. In QML, data

*ssa5517@psu.edu

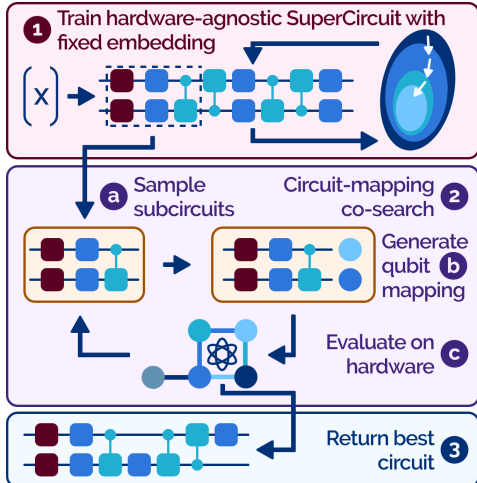


Figure 2: QuantumNAS: A state-of-the-art QCS framework.

must be embedded into *data embedding* gates, the choices and locations of which impact circuit performance. At the algorithm level, QML cannot compute gradients efficiently via automatic differentiation as intermediate states cannot be copied [89] and collapse on measurement [52]. Instead, QML uses methods like parameter-shift rules [71] that scale poorly with problem size. At the compilation level, mapping classical neural networks with arbitrary topology onto memory is expensive due to efficient data movement. However, due to the limited connectivity of NISQ devices, large routing costs are incurred when QML circuits do not match device topology.

Existing QCS methods naively adopt classical ML designs, precluding compatibility with the unique constraints of QML. We explain these mismatches using QuantumNAS [80], a state-of-the-art QCS method. As shown in Fig. 2, QuantumNAS first trains a large device-agnostic *SuperCircuit* with fixed data embeddings. Next, it performs an evolutionary co-search to identify a performant and noise-robust circuit-qubit mapping pair, using the trained *SuperCircuit* parameters to estimate the performance of candidate circuits on the target device. Finally, it returns the best circuit-qubit mapping pair found. Other frameworks such as QuantumSupernet [18] follow similar designs, and thus also experience the following issues:

1. They use device-agnostic search spaces, necessitating an additional search for logical-to-physical qubit mappings. The found mappings are also hardware-inefficient, since selected circuits usually do not match the device topology and SWAP gates must be inserted before circuit execution.
2. They do not assess the impact of data embeddings on circuit performance as they use fixed, dataset-agnostic data embeddings. This leads to circuits with poor performance.
3. They adopt strategies from classical ML relying heavily on gradient computation, which is expensive on quantum computers and scales poorly with circuit size.
4. They perform expensive performance evaluation for all circuits. This is inefficient, since many circuits have extremely

low fidelity, and will perform poorly since their outputs will be severely corrupted by to device noise. Existing methods do not have any mechanisms to identify and eliminate the performance evaluation for such circuits.

Consequently, existing QCS frameworks incur significant search overheads even for small circuits and problem sizes, and often perform poorly on QML tasks.

To address the problems above, we propose *Élivágar*, a resource-efficient, high-performance QCS framework tailored to QML systems. **First**, *Élivágar* uses a device topology- and noise-aware circuit generation process to generate noise robust circuits that are hardware efficient, eliminating the costly circuit-mapping co-search (issue 1). **Second**, to mitigate performance bottlenecks caused by fixed, data-agnostic data embeddings (issue 2), *Élivágar* generates circuits with different data embeddings and variational gates, allowing *Élivágar* to search for the optimal data embedding for a QML task. **Third**, to reduce the overheads of training-based circuit evaluations (issue 3), *Élivágar* introduces a novel, cheap-to-compute performance predictor, *representational capacity*, for circuit performance evaluation. By using *representational capacity*, *Élivágar* eliminates the expensive training step in the QCS workflow while still effectively predicting circuit performance. **Last**, *Élivágar* makes use of the insight that evaluating noise robustness is much simpler than evaluating performance. By introducing *Clifford noise resilience*, a predictor of circuit noise robustness, it decouples these two evaluations to enable early rejection of low-fidelity circuits (issue 4).

Our evaluations using 9 near-term QML benchmarks show that *Élivágar* finds circuits with 5.3% higher accuracy while being $271\times$ faster than prior state-of-the-art QCS methods. Moreover, we show that the speedup of *Élivágar* increases with problem size. In summary, our contributions are:

1. We propose a novel QCS workflow, *Élivágar*, that is tailored to QML systems and addresses the design flaws in current classically-inspired QCS methods.
2. We show that noise-guided, topology-aware and data embedding-aware circuit search, on average, leads to a 5.3% improvement in circuit performance compared to current methods.
3. We show that by using *representational capacity* to predict circuit performance, the number of circuit executions in *Élivágar* can be improved by $22\times$ - $523\times$ relative to training-based evaluation strategies.
4. We show that by performing early rejection of low-fidelity circuits using *Clifford noise resilience*, the resource efficiency of *Élivágar* can be further improved by $2\times$ - $20\times$ depending on noise level.

We open source *Élivágar* to facilitate future QCS research at <https://github.com/SashwatAnagolum/Elivagar>.

2. Background and Motivation

2.1. Executing quantum programs on NISQ computers

NISQ-era devices with limited qubit connectivity and imperfect operations make program executions error-prone. Operations on non-adjacent qubits are enabled using SWAPs, as shown in Fig. 3a, which are usually implemented using three 2-qubit gates, making them noisy and expensive. Prior works [15, 35, 48, 67, 78] show that circuit fidelity can be improved through circuit compilation techniques such as *qubit mapping and routing*, which minimize SWAPs, making it desirable to eliminate SWAPs to make circuits hardware-efficient and boost circuit fidelity.

2.2. Variational circuits for QML

Variational circuits in QML consist of data embedding gates, trainable variational gates, and measurement operations. The data embedding gates are used to transform classical data into quantum states by using these classical data as rotation angles for the data embedding gates. Once the data has been embedded, the variational gates in the circuit are used to manipulate the representations of the data, and measurements are applied by using measurement operators to extract classical data for post-processing, such as for computing parameter updates during training, or for making predictions during inference.

After training, a QML circuit can be used for inference. To do so, we embed into the circuit the data to make predictions based on, and use the learned parameter values for the variational gates. The circuit is executed on a quantum device, and measurements are performed to extract classical data which can be post-processed to obtain predictions. The post-processing can potentially involve statistical analysis, decoding, or other task-specific operations transforming measurement outputs into meaningful results.

Different circuits can be constructed by varying the number, type, and placement of gates used. Due to the large search space, designing performant QML circuits is challenging. As a result, practitioners often rely on a set of commonly used variational *templates*, such as the hardware efficient ansatz [45]. However, numerous works [9, 12, 28, 45] show that these templates tend to perform poorly on QML tasks as circuit size increases, motivating the search for better circuit structures.

2.2.1. Data embedding gates

The choice of data embedding in a QML circuit significantly impacts its performance, as highlighted in prior studies [10, 62, 72, 73]. To illustrate, consider the example in Fig. 3b, where two circuits share the same variational gates, but differ in data embeddings (RX(x) and RY(x), versus RX(x) alone), resulting in markedly different performance outcomes. However, choosing a suitable data embedding for a given QML task is challenging due to the vast search space, leading many QML circuits to use a fixed embedding such as an angle [7] or Instantaneous Quantum Polynomial-time (IQP)

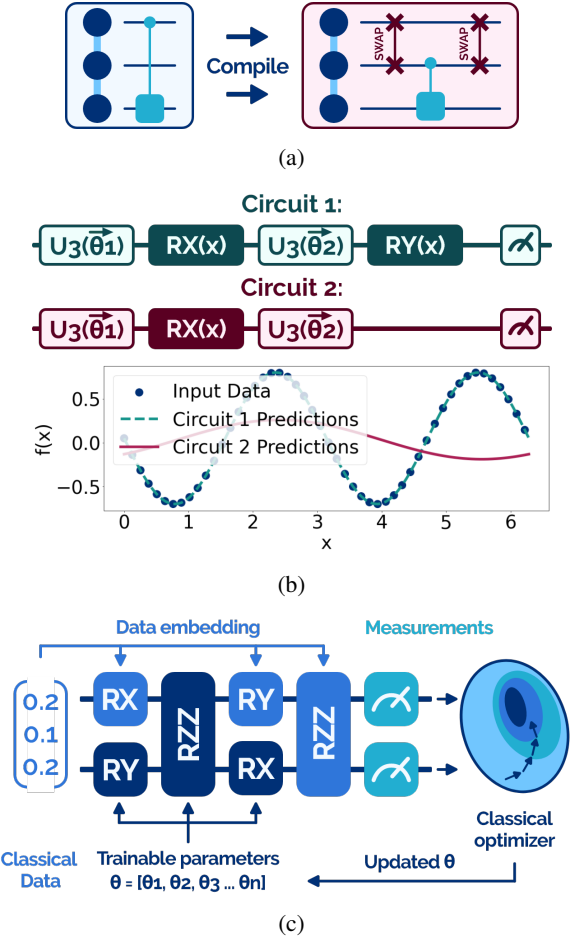


Figure 3: (a) Circuit and device topology mismatch results in a large routing cost due to noisy SWAP gates. (b) Both circuits use the same trainable gates, but different data embeddings. Circuit 1 learns the target function $f(x)$ but Circuit 2 fails, highlighting the importance of suitable data embeddings for QML tasks. (c) QML circuits consist of data embedding gates, trainable gates, and measurement operations. QML training involves running circuits on a quantum device and tuning parameters using a classical optimizer.

embedding [24], regardless of the nature of the QML task. This often results in suboptimal performance due to the mismatch between the embedding used and the QML task.

2.2.2. Training variational circuits

Variational circuits are trained using gradient-based optimization in a classical-quantum feedback loop, as shown in Fig. 3c. However, training variational circuits is costlier than training classical ML models. In classical ML, gradients are efficiently computed via Automatic Differentiation (AD) [4], which takes constant time. However, this approach is not feasible on quantum computers since intermediate quantum states cannot be manipulated or copied due to the no-cloning theorem [52, 89]. Thus, alternative methods such as parameter-shift rules [71, 87] are used. Parameter-shift methods compute the gradient of a single parameter θ by running two circuits

Table 1: Key differences between Élivágar and existing QCS methods. ES, RL, and MCTS refer to evolutionary search (ES), reinforcement learning (RL), and Monte Carlo tree search (MCTS), respectively.

Framework	Search Space	Search Algorithm	Candidate Evaluation Strategy	Runtime Bottleneck
MCTS-QAOA [91]	Pauli strings	RL + MCTS	Train circuit	Sample-inefficient RL
QCEAT [30]	Random circuits	ES	Train circuit	Gradient computation
QuantumSupernet [18]	SuperCircuit	Random search	SuperCircuit loss	Gradient computation
QuantumNAS [80]	SuperCircuit	ES	SuperCircuit loss	Gradient computation
Élivágar	Device- and noise-aware circuits	Noise-guided random search (Sec. 4)	CNR (Sec. 5) and RepCap (Sec. 6)	—

with shifted parameters, $\theta + s$ and $\theta - s$ (where s is a constant), and then computing the difference. Unfortunately, this method requires circuit executions scaling linearly with the number of circuit parameters, in contrast to the constant scaling of AD methods; thus, QML gradient computation scales poorly with the number of parameters.

2.3. Limitations of existing QCS works

QCS works that use reinforcement learning (RL), such as MCTS-QAOA [91], converge slowly due to the large action and state spaces involved in quantum circuit design, and incur large circuit evaluation costs during training of the RL model. SuperCircuit-based works such as QuantumSupernet [18] and QuantumNAS [80] also result in impractical runtime overheads due to the high cost of SuperCircuit training (Section 2.2.2). These methods additionally require a circuit-mapping co-search which is often unable to make circuits hardware-efficient, leading to SWAP insertions and reduced circuit noise robustness (Section 2.1). Moreover, SuperCircuit-based works cannot search for optimal data embeddings for a QML task, leading to lowered performance due to data embedding-QML task mismatch (Section 2.2.1). Together, these issues hinder the ability of existing works to find performant circuits while maintaining low search costs.

2.4. The necessity of a new QCS pipeline

It is infeasible to improve significantly on existing QCS works since many of the prerequisites for performant, low-cost QCS are fundamentally incompatible with SuperCircuit-based methods. For example, SuperCircuit training is necessary for accurate circuit performance prediction, preventing the elimination of training and gradient computation. However, gradient computation on quantum hardware is costly, leading to high search overheads. Additionally, SuperCircuit performance prediction is only accurate when using a fixed data embedding for all

candidate circuits, precluding the possibility of searching for optimal data embeddings to boost performance.

Therefore, to enable efficient QCS, it is necessary to develop a novel QCS pipeline that accounts for the constraints of QML systems and NISQ-era quantum hardware. To this end, we propose Élivágar, a QCS framework which eschews using a SuperCircuit in favor of training-free predictors of circuit performance, avoiding the training-induced runtime bottlenecks of prior work. Moreover, since Élivágar does not use a SuperCircuit, it can search for optimal data embeddings and perform efficient noise-guided candidate sampling, allowing it to generate hardware-efficient circuits at negligible cost and outperform prior QCS works consistently. Élivágar’s key differences with prior QCS works are presented in Table 1.

3. Overview of Élivágar

As illustrated in Fig. 4, Élivágar consists of five steps:

- 1. Topology- and noise-aware candidate circuit generation:** First, Élivágar generates candidate circuits and data embeddings in a device- and noise-aware manner.
- 2. Evaluation of noise robustness:** Élivágar then computes the Clifford noise resilience score for circuits to estimate circuit noise robustness.
- 3. Early rejection of low-fidelity circuits:** Élivágar ranks candidate circuits based on their Clifford noise resilience and eliminates low-fidelity circuits.
- 4. Evaluation of circuit performance:** Élivágar predicts the performance of the remaining circuits on the target QML task using representational capacity.
- 5. Final circuit selection:** Finally, Élivágar computes composite scores combining representational capacity and Clifford noise resilience for the remaining candidate circuits, and returns the best circuit.

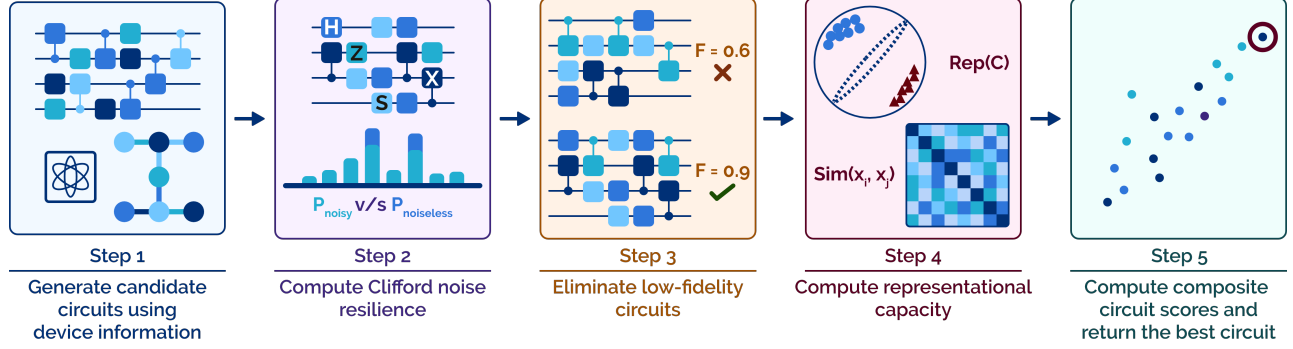


Figure 4: An overview of Élivágar.

We break Élivágar down into three parts — candidate circuit generation (step 1, Section 4), noise-guided candidate rejection (step 2-3, Section 5), and circuit performance estimation and circuit selection (step 4-5, Section 6).

4. Candidate circuit generation

To overcome the issues of SuperCircuit-based circuit generation discussed in Section 1, Élivágar directly generates candidate circuits and data embeddings based on target device topology via a noise-guided sampling policy shown in Algorithm 1. This approach has the following advantages over SuperCircuit-based methods: 1) generating circuits based on device topology ensures hardware-efficiency and improves circuit fidelity; 2) circuits are generated along with optimal qubit mappings, eliminating the need for an expensive circuit-mapping co-search; 3) noise-guided sampling further boosts the average fidelity of candidate circuits; 4) generating varied data embeddings for candidate circuits improves selected circuit performance.

As a result, circuits generated by Élivágar have 18.9% higher fidelity than device-unaware circuits optimized using SABRE [35] (Section 9.1). Furthermore, Élivágar obtains 6% higher accuracy on average when searching for data embeddings than when using a fixed data embedding (Section 9.3).

4.1. Noise-guided candidate circuit generation

As shown in Algorithm 1, Élivágar first chooses a connected subgraph from the device topology, and then samples a list of gates to form the circuit. Gate placement choices are guided by subgraph connectivity, noise information such as qubit coherence times, 1- and 2-qubit gate fidelities, readout fidelities, and the current circuit structure. Following prior works in classical NAS [17, 38], Élivágar samples qubits and gate placements from probability distributions instead of directly choosing the best options to encourage candidate diversity.

Choosing a subgraph $S(V^{(S)}, E^{(S)})$ for every circuit allows Élivágar to trivially obtain a qubit mapping for every generated circuit by using $V^{(S)}$. This way, Élivágar avoids the expensive circuit-mapping co-search required by other QCS frameworks. In contrast, the evolutionary co-search used by QuantumNAS [80] cannot guarantee hardware-efficiency, and

Algorithm 1: Generate device-aware circuits

Input: Device topology graph $G(\{V_i\}, \{E_j\})$; Qubit readout errors $\{R_i\}$; Qubit coherence times $\{T1_i\}, \{T2_i\}$; 2-qubit gate fidelity $\{Q_e\}$; Output circuit configuration O_{conf} .

Output: Candidate circuit C .

- 1 Sample a set of connected subgraphs $\{S_i\}$ with $V^{(S_i)} = O_{\text{conf}} \cdot n_q \forall_i$ from G ;
 - 2 Select a subgraph $S(V^{(S)}, E^{(S)})$ from distribution $P_{\{S_i\}}(S | R_{V^{(S)}}, T1_{V^{(S)}}, T2_{V^{(S)}}, Q_{E^{(S)}})$;
 - 3 Initialize C as an empty circuit;
 - 4 Randomly sample a list L_{op} of 1-qubit and 2-qubit gates based on $O_{\text{conf}} \cdot n_{\text{params}}$ and $O_{\text{conf}} \cdot n_{\text{embeds}}$;
 - 5 **for** op in L_{op} **do**
 - 6 **if** op is a 1-qubit gate **then**
 - 7 Select a qubit $q \in V^{(S)}$ from distribution $P_{1q}(q | C, T1_q, T2_q)$;
 - 8 Append $op(q)$ to C ;
 - 9 **if** op is a 2-qubit gate **then**
 - 10 Select an edge $e = (q_0, q_1) \in E^{(S)}$ from $P_{2q}(e | C, T1_{q_0}, T1_{q_1}, T2_{q_0}, T2_{q_1}, Q_e)$;
 - 11 Append $op(q_0, q_1)$ to C ;
 - 12 Select a set q_{meas} of $O_{\text{conf}} \cdot n_{\text{meas}}$ qubits in $V^{(S)}$ from distribution $P_{\text{meas}}(q | R_{E^{(S)}})$;
 - 13 Append MEASURE(q_{meas}) to C ;
 - 14 Randomly designate $O_{\text{conf}} \cdot n_{\text{embeds}}$ parametric gates in C for use as data embedding gates;
 - 15 **return** C ;
-

is very expensive: eliminating it results in Élivágar becoming $1.4 \times -33.4 \times$ faster (Section 9.4). Thus, rather than use an alternative co-search mechanism, Élivágar adopts a novel approach that completely eliminates the need for a co-search, resulting in higher circuit fidelity and search efficiency.

Insight 1: Generating device-aware circuits

Generating device- and noise-aware circuits eliminates the need for an expensive circuit-mapping co-search, improves circuit fidelity, and ensures hardware-efficiency.

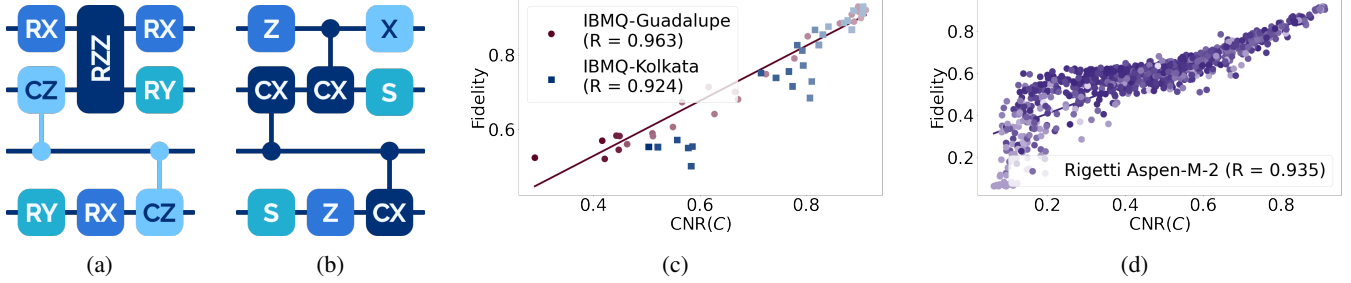


Figure 5: (a) A circuit and (b) a Clifford replica of the circuit. CNR is strongly correlated with circuit fidelity, as demonstrated using circuits run on (c) IBMQ-Kolkata and IBMQ-Guadalupe, and a (d) noise model of Rigetti Aspen-M-2.

4.2. Generating data embeddings

Élivágar employs a simple strategy to generate data embeddings: a few gates in each circuit are used as data embedding gates, with each gate randomly assigned one dimension of the input data to embed (line 14 in Algorithm 1). Despite the random generation of data embeddings, Élivágar leverages representational capacity (Section 6) to predict circuit performance with different data embeddings and select circuits that contain the most suitable data embeddings for the QML task of interest. Consequently, Élivágar optimizes both the data embedding and the variational gates in the selected circuit, resulting in improved performance. By co-searching for data embeddings and variational gates, Élivágar unlocks 6% higher accuracy than when using a fixed data embedding (Section 9.3).

Insight 2: Searching for optimal data embeddings

Using optimized data embeddings significantly boosts performance over QCS methods with fixed embeddings.

5. Noise-guided candidate rejection

A key insight of Élivágar is that predicting circuit noise robustness is much simpler than predicting circuit performance. Leveraging this, Élivágar reduces the number of performance estimations required by identifying and discarding low-fidelity circuits. To do so, Élivágar defines a predictor, *Clifford noise resilience* (CNR), that accurately predicts circuit fidelity.

While simulating a quantum circuit is exponentially costly in general, Clifford circuits are a class of efficiently simulable quantum circuits [8]. Thus, the fidelity of Clifford circuits can be calculated efficiently by comparing their outputs with noiseless classical simulation results. This enables efficient fidelity estimation for a circuit by using the fidelity of its *Clifford replicas* as a proxy [32], which is expensive to compute directly for large circuits due to the high simulation cost. While prior works use Clifford replicas to create circuit compilation passes [14, 15, 68] and characterize device noise [67], Élivágar uses Clifford circuits to identify noise-robust circuits for QML. First, we elaborate on Clifford replicas and CNR, and then show the strong correlation between CNR and circuit fidelity.

5.1. Creating Clifford replicas

Clifford replicas of a circuit are created by substituting all of the non-Clifford gates in the circuit with Clifford gates. Previous works such as [14, 15] generate a Clifford replica for a circuit by substituting non-Clifford gates with the closest Clifford gate as measured by the diamond norm. In contrast, Élivágar uses multiple Clifford replicas with randomly chosen Clifford gates. The primary reason for this is that prior works deal with circuits at the compilation stage, where the parameter values to be used with each gate are known. In contrast, since Élivágar generates Clifford replicas for circuits before training, it is impossible to know what parameter values will be used with the circuit. Moreover, since gate angles will be changed due to training or different input data, using multiple Clifford replicas, each with randomly chosen Clifford gates, provides a reliable measure of circuit noise robustness over the course of training and prediction.

Figure 5a and 5b show a circuit and one of its Clifford replicas. Since Clifford replicas use the same structure as the original circuit, circuit properties such as depth, are preserved. Élivágar creates multiple Clifford replicas and averages the fidelities of all the constructed replicas. We find that using as few as 16 Clifford replicas can accurately characterize circuit noise robustness.

5.2. Computing CNR

To compute the CNR for a circuit, Élivágar first collects the noisy outputs P_{noisy} obtained by executing the generated Clifford replicas on the target quantum device. Then, it obtain the ideal Clifford replica outputs $P_{\text{noiseless}}$ via simulation. Élivágar then calculates the Total Variation Distance (TVD) between the noisy and noiseless outputs and computes the fidelity as $\text{Fid} = 1 - \text{TVD}$:

$$\text{TVD} = \frac{1}{2} \sum_{i \in [2^q]} |P_{\text{noiseless}}(|i\rangle) - P_{\text{noisy}}(|i\rangle)|. \quad (1)$$

$\text{CNR}(C)$, the Clifford noise resilience for circuit C , is defined as the average fidelity of the M Clifford replicas $C_R(i)$:

$$\text{CNR}(C) = \frac{1}{M} \sum_{i=1}^M \text{Fid}(P_{\text{noiseless}}^{C_R(i)}, P_{\text{noisy}}^{C_R(i)}). \quad (2)$$

5.3. Candidate circuit rejection

After computing the CNR of candidate circuits, Élivágar ranks circuits by CNR and by default rejects circuits with CNR values less than a threshold of 0.7, or outside the top 50% of all candidates. However, these values can be set by users of Élivágar as hyperparameters. All rejected circuits require no performance evaluation, leading to reduced resource requirements. Depending on device noise levels and threshold values, this rejection step can speed up Élivágar significantly. For example, when searching for a 250-parameter circuit on IBMQ-Manila with a CNR threshold of 0.9, Élivágar can reject 95% of circuits, achieving an almost 20x reduction in circuit executions.

In comparison, SuperCircuit-based QCS works conflate the evaluation of circuit noise robustness and circuit performance, making the identification of low-fidelity circuits unnecessarily expensive. In these methods, the performance of a candidate circuit is evaluated using a validation data set $\mathcal{X}_{\text{valid}}$ on the target device. This requires executing $|\mathcal{X}_{\text{valid}}|$ circuits to evaluate every candidate circuit. This cost is often significantly larger than the constant number of circuits required to compute CNR, making identifying low performing circuits needlessly costly in SuperCircuit-based frameworks.

Figure 5c and 5d show the correlation between the CNR and the fidelity of circuits executed on IBMQ-Guadalupe and IBMQ-Kolkata, and a noise model of Rigetti Aspen-M-2. In all cases, CNR is highly predictive of circuit fidelity.

Insight 3: Early rejection of low-fidelity circuits

Noise robustness evaluation is simpler than performance evaluation. Evaluating noise robustness first using Clifford noise resilience enables early rejection of low-fidelity circuits, reducing evaluation costs.

6. Circuit performance evaluation

Our calculations indicate that over 90% of the circuit executions for SuperCircuit-based QCS methods are performed during SuperCircuit training, due to the high cost of computing gradients on quantum hardware via the parameter-shift rule. Thus, eliminating the initial training phase of QCS is crucial for resource efficiency.

Élivágar addresses this by introducing a novel, cheap-to-compute circuit performance predictor, *representational capacity* (RepCap). RepCap requires far fewer circuit executions than training-based evaluation strategies, but is just as effective at predicting circuit performance. Fig. 6 shows the correlations of SuperCircuit predicted losses and RepCap with trained circuit performance on the FMNIST-2 task. Despite not requiring any training, RepCap is as strong a predictor of performance as a trained SuperCircuit. RepCap is a strong predictor of circuit performance on other QML benchmarks as well, as shown in Fig. 7, and has a Spearman R correlation of 0.632

with circuit performance over all the QML benchmarks used for evaluation.

First, we define RepCap and provide some intuition about it, and then elaborate on how to compute RepCap. Then, we discuss how we combine CNR and RepCap to rank the circuits remaining after the noise-guided circuit elimination process.

6.1. Predicting circuit performance using RepCap

Intuitively, RepCap measures the intra-class similarities and inter-class separation of the final quantum states for a variational circuit. As illustrated in Fig. 6a, the larger the inter-cluster distance and the smaller the intra-cluster distance in the final qubit state space, the higher the RepCap of a variational circuit is. A higher RepCap indicates that the circuit has a larger “capacity” for representing the input data, and likely will perform better.

RepCap for circuit C is defined as:

$$\text{RepCap}(C) = 1 - \frac{\|R_C - R_{\text{ref}}\|_2^2}{2 \cdot n_c \cdot d_c^2}, \quad (3)$$

where d_c and n_c are the number of samples selected from each class and the number of classes in $\mathcal{X}_{\text{train}}$, respectively. $\|\cdot\|_2$ is the Frobenius norm. R_{ref} is a $d \times d$ reference matrix that captures the ideal circuit behaviour, i.e. $R_{\text{ref}}(i, j) = 1$ iff $y_i = y_j$, and $R_{\text{ref}}(i, j) = 0$ otherwise. R_C is a $d \times d$ matrix that captures pairwise similarities between the representations of data points x_i and x_j created by circuit C , with $R_C(i, j) \in [0, 1]$.

The entries of R_C used in Eq. (3) are the *induced similarity* IS_C between data points x_i and x_j , i.e.,

$$R_C(i, j) = \text{IS}_C(x_i, x_j). \quad (4)$$

$\text{IS}_C(x_i, x_j)$ is defined as the averaged similarity of the output quantum states $\rho_C(x_i, \theta)$ and $\rho_C(x_j, \theta)$ of circuit C when fed input data x_i and x_j over random parameters θ . In practice, we use classical approximations $\hat{\rho}_C(x_i, \theta)$, computed via Algorithm 2, instead of states $\rho_C(x_i, \theta)$ in order to avoid executing circuits for every pair of samples x_i and x_j :

$$\text{IS}_C(x_i, x_j) = \frac{1}{n} \sum_{\theta=\theta_1}^{\theta_n} \text{Sim}(\hat{\rho}_C(x_i, \theta), \hat{\rho}_C(x_j, \theta)) \quad (5)$$

The angles $\{\theta_i\}$ can be uniformly sampled. Then the *similarity* $\text{Sim}(x_i, x_j)$ between x_i, x_j can be defined as the one minus Total Variational Distance (TVD) between their output states by C using a randomized measurement protocol [19, 23, 29],

$$\text{Sim}(\hat{\rho}_C(x_i, \theta), \hat{\rho}_C(x_j, \theta)) = \frac{1}{n_{\text{bases}}} \sum_{k=1}^{n_{\text{bases}}} 1 - \text{TVD}(\hat{\rho}_C(x_i, \theta)_k, \hat{\rho}_C(x_j, \theta)_k). \quad (6)$$

where n_{bases} is the number of random bases we use to approximate the two states.

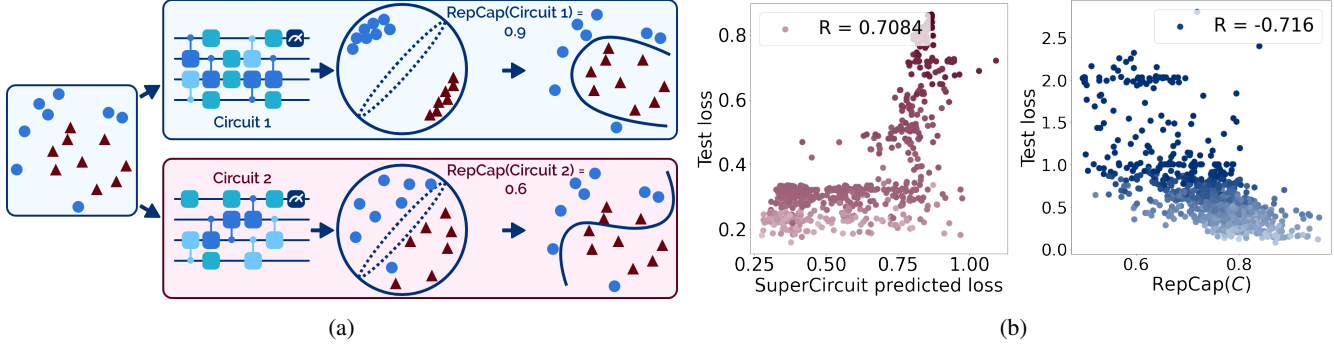


Figure 6: (a) Representational capacity measures the degree of intra-class similarity and inter-class separation of the quantum states created by a circuit. Circuit 1 has a higher representational capacity, and so is likely to perform better than Circuit 2. (b) Predicting circuit performance on the FMNIST-2 benchmark. RepCap predicts circuit performance as well as a SuperCircuit, despite not involving gradient computation.

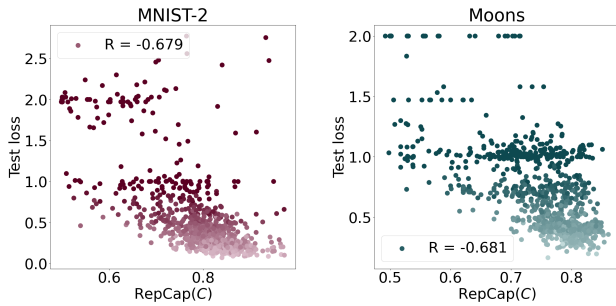


Figure 7: Representational capacity is a strong predictor of performance for various QML tasks.

Algorithm 2: Constructing the classical approximation $\hat{\rho}_C(x, \theta)$ of a representation $\rho_C(x, \theta)$

Input: Circuit C ; Input data x ; variational parameters θ ; array of random rotation angles α of size $n_{\text{bases}} \times n_{\text{meas}} \times 3$.

Output: Classical approximation $\hat{\rho}_C(x, \theta)$ of $\rho_C(x, \theta)$

- 1 Append a set of n_{meas} U3 gates to C acting on the n_{meas} qubits being measured;
 - 2 Initialize $\hat{\rho}_C(x, \theta)$ as an empty list of length n_{bases} ;
 - 3 **for** $i = 1$ **to** n_{bases} **do**
 - 4 Execute circuit $C(x, [\theta, \alpha_i])$;
 - 5 Construct probability distribution $P_{(\alpha_i)}(x, \theta)$ using the outputs of $C(x, [\theta, \alpha_i])$;
 - 6 Set $\hat{\rho}_C(x, \theta)_i \leftarrow P$
 - 7 **return** $\hat{\rho}_C(x, \theta)$;
-

Computing RepCap requires only $n_c \cdot d_c \cdot n_p$ circuit executions, where n_p is the number of parameter initializations we average over. In practice, we take $d_c = 16$, $n_p = 32$. For N_C circuits, Élivágar then requires $512 \cdot N_C \cdot n_c$ executions. In contrast, SuperCircuit-based methods require $2 \cdot t \cdot |\mathcal{X}_{\text{train}}| \cdot \bar{p} + N \cdot |\mathcal{X}_{\text{valid}}|$ circuit executions to train a SuperCircuit for t epochs via sampling subcircuits with \bar{p} parameters each on average, and then evaluate the performance of N subcircuits. The initial training overhead of a SuperCircuit scales very poorly with problem size due to the high cost of gradient

computation, increasing the speedup of Élivágar with problem size. For example, Élivágar is only $44\times$ faster than QuantumNAS on the 16-parameter Moons task (Section 7); for the 72-parameter MNIST-10 task, the speedup is over $5000\times$.

Insight 4: Predict circuit performance without training

By analyzing the output states of a circuit for different input data, we can cheaply estimate circuit performance as well as prior work.

6.2. Final evaluation of remaining circuits

Élivágar combines $\text{CNR}(C)$ and $\text{RepCap}(C)$ to accurately predict performance of the remaining circuits on the target device. The composite score $\text{Score}(C)$ for circuit C is given by

$$\text{Score}(C) = \text{CNR}(C)^{\alpha_{\text{CNR}}} \times \text{RepCap}(C). \quad (7)$$

α_{CNR} is a hyperparameter controlling the relative importance of $\text{CNR}(C)$, with $\text{RepCap}(C)$ and $\text{CNR}(C)$ being equally important at $\alpha_{\text{CNR}} = 1$. For all experiments, we set $\alpha_{\text{CNR}} = 0.5$. Finally, Élivágar returns the circuit with the highest $\text{Score}(C)$.

7. Experimental Setup

7.1. Benchmarks

We conduct experiments on 9 different QML benchmarks. A summary of the benchmarks is shown in Table 2. Train and Test in Table 2 refer to the number of samples used for training and testing, respectively. Params is the number of parameters in the circuits we search for in Section 8. Moons is a synthetic dataset generated using scikit-learn. We select a balanced subset of the original Bank dataset [43]. We use classes $\{0, 1\}$ from the MNIST dataset for MNIST-2, $\{0, 1, 4, 8\}$ for MNIST-4, $\{\text{T-shirt, Trouser}\}$ from the FMNIST dataset for FMNIST-2, and $\{\text{T-shirt, Trouser, Bag, Ankle Boot}\}$ for FMNIST-4. For the MNIST and FMNIST benchmarks, we center crop the original images to 24×24 and downsample them to 4×4 using mean pooling, except for MNIST-10, which is downsampled to 6×6 .

Table 2: Summary of the 9 QML benchmarks used for evaluations.

Benchmark	Classes	Data Dim.	Train	Test	Params
Moons	2	2	0.6K	0.12K	16
Bank	2	4	1.1K	0.12K	20
MNIST-2	2	4x4	1.6K	0.4K	20
MNIST-4	4	4x4	8K	2K	40
FMNIST-2	2	4x4	1.6K	0.2K	32
FMNIST-4	4	4x4	8K	2K	24
Vowel-2	2	10	0.6K	0.12K	32
Vowel-4	4	10	0.6K	0.12K	40
MNIST-10	10	6x6	60K	10K	72

Table 3: Summary of the *real quantum hardware used*.

Device	Qubits	QV	Median Error Rate ↓		
			Readout	1Q	2Q
OQC Lucy	8	–	1.3e-1	6.2e-4	4.4e-2
Rigetti Aspen M-3	79	–	8.0e-2	1.5e-3	9.3e-2
IBMQ Jakarta	7	32	2.6e-2	2.2e-4	8.5e-3
IBMQ Nairobi	7	32	2.4e-2	2.7e-4	9.6e-3
IBMQ Lagos	7	32	1.9e-2	2.1e-4	9.8e-3
IBMQ Perth	7	32	2.8e-2	2.8e-4	8.7e-3
IBMQ Geneva	16	32	2.7e-2	2.2e-4	1.1e-2
IBMQ Guadalupe	16	32	2.0e-2	2.9e-4	8.9e-3
IBMQ Kolkata	27	128	1.2e-2	2.3e-4	9.0e-3
IBMQ Mumbai	27	128	1.9e-2	2.0e-4	9.6e-3
IBMQ Kyoto	127	–	1.4e-2	2.5e-4	9.1e-3
IBMQ Osaka	127	–	1.7e-2	2.2e-4	1.0e-2

The Vowel-2 and Vowel-4 datasets are constructed by merging 8 out of the 9 classes in the original Vowel dataset, and selecting the 10 most significant PCA dimensions.

7.2. Backends and compiler configurations

The hardware devices used are listed in Table 3. We also use multiple noisy simulators use noise models based on IBM Nairobi, IBM Lagos, IBM Perth, IBMQ Jakarta, IBM Guadalupe, Rigetti Aspen-M-2, Rigetti Aspen-M-3, and OQC Lucy in order to perform evaluations, compute circuit fidelity and CNR. To compute RepCap and perform circuit training, we use noiseless simulators from PennyLane [6] and TorchQuantum [80]. Before running circuits on any hardware device or noisy simulator, we compile the circuit using the default Qiskit compiler with optimization level set to 3 for all competing methods except for QuantumNAS, for which we use level 2, and Élivágar, for which we use level 0.

7.3. Training methodology

All circuits are trained using the same methodology to ensure fair comparisons. We train circuits for 200 epochs using a

batch size of 128 and optimize parameters using the Adam optimizer with learning rate 0.01. No weight decay or learning rate scheduling is used. The training objective is to minimize the classification loss between circuit predictions and the labels of the training set. We perform training on noiseless simulators using the TorchQuantum package [80], and use an AWS ml.g4dn.xlarge instance with 16GB of memory and an NVIDIA T4 GPU.

7.4. Competing methods

We compare Élivágar to four competing methods. Every circuit compared to, including those chosen by Élivágar, all contain the same number of parameters in order to ensure a fair comparison. The number of parameters used in the circuits for each benchmark is given in Table 2.

Random: we randomly generate 25 circuits using the RXYZ + CZ gateset from [80], and report the average performance of the circuits.

Human designed (baseline): We use three data embedding schemes (angle, amplitude, and IQP embedding) paired with paired with the commonly used BasicEntanglerLayers template from the PennyLane [6] library. We train all three circuits and report the average performance.

QuantumSupernet [18]: We modify the SuperCircuit training procedure proposed in [18] and use mini-batch gradient descent with batch size 32 instead of full-batch gradient descent to ensure all SuperCircuit parameters are updated sufficiently. All other hyperparameters are taken from [18].

QuantumNAS [80]: We use the same hyperparameters for SuperCircuit training and evolutionary search as [80], and use the RXYZ + CZ gateset since it performs the best out of the 6 gatesets in [80] before pruning. We do not perform iterative pruning for trained QuantumNAS circuits as the pruning phase does not contribute towards circuit search.

7.5. Hyperparameters for Élivágar

We randomly sample $d_c = 16$ data points from each class of $\mathcal{X}_{\text{train}}$ and $n_p = 32$ parameter initializations to compute RepCap. We use $M = 32$ Clifford replicas to compute CNR, and reject circuits with CNR scores less than 0.7 or outside the top 50%. We construct composite scores using $\alpha_{\text{CNR}} = 0.5$. To mitigate the effects of random circuit sampling, we repeat our workflow 25 times, and report the average performance.

7.6. Figure of merit

We measure the performance of a circuit using the classification accuracy it obtains over a dedicated test set for each benchmark. We highlight the difference between circuit accuracy and circuit fidelity in this work: the classification accuracy of a circuit is the fraction of predictions made by the circuit that are correct, i.e. match the ground truth label of the associated sample for which the prediction was made; while fidelity measures the degree to which the outputs of a quantum circuit remain unaffected by hardware noise.

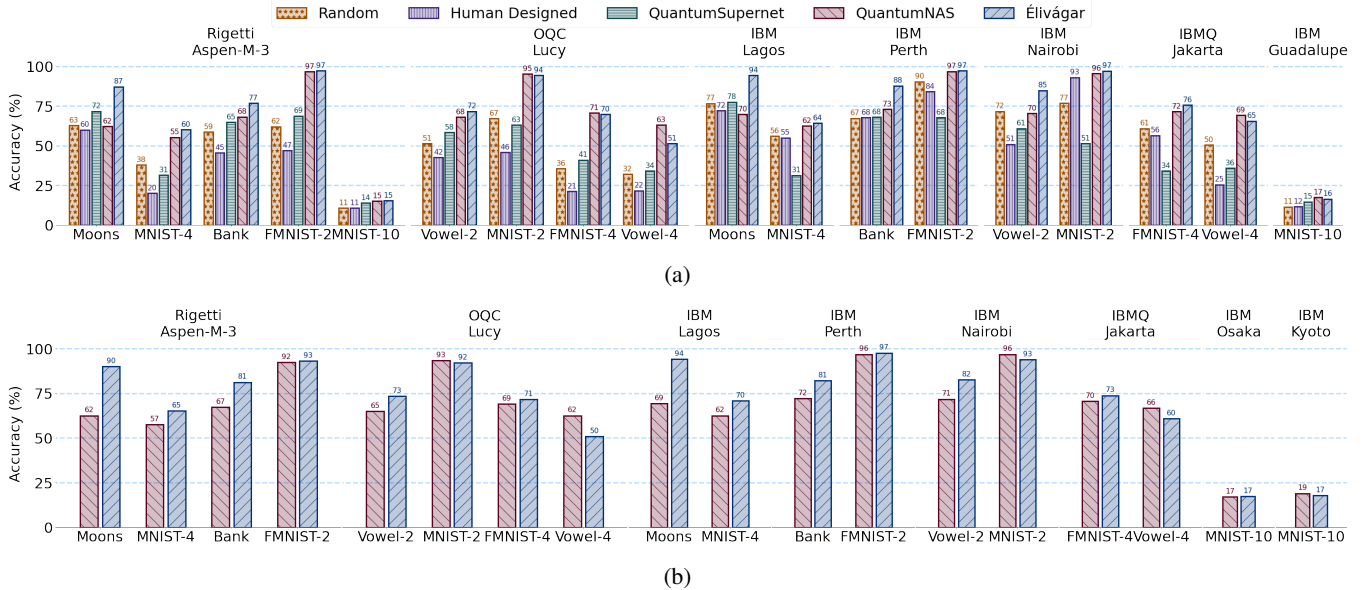


Figure 8: Results using (a) *noisy simulations* with different noise models (each bar shows the mean of 25 runs), and (b) *real quantum hardware* accessed via Amazon Braket and IBM Quantum. All plots show absolute classification accuracy (*higher is better*).

8. Results

8.1. Performance on QML benchmarks

Fig. 8a shows performance on 9 different QML benchmarks, using *noisy simulators* with noise models of Rigetti Aspen-M-3, OQC Lucy, IBM Lagos, IBM Perth, IBM Nairobi, IBMQ Jakarta. Fig. 8b shows the results of evaluations performed on *real quantum hardware*. *Élivágar* is competitive with or outperforms QuantumNAS on all benchmarks except Vowel-4. Circuit performance on the Rigetti Aspen-M-3 and OQC Lucy devices is worse than on the IBM devices due to their higher noise levels (see Table 3). On average, *Élivágar* achieves 5.3% higher accuracy than QuantumNAS, and 22.6% higher accuracy than the human designed baseline.

8.2. Runtime speedups

We consider two hardware setups when measuring the speedup of *Élivágar* over QuantumNAS, which we elaborate on below.

8.2.1. Using classical simulators

Using classical simulators results in reduced training costs as gradients can be computed efficiently using backpropagation. Additionally, training and inference on noiseless simulators can be performed in a batched manner, further speeding up the QCS process. We provide absolute runtime values for both QuantumNAS and *Élivágar* in Table 4. Even when using classical simulators and backpropagation, which disproportionately benefits training-heavy frameworks such as QuantumNAS, *Élivágar* is 11.7 \times faster than QuantumNAS on average. Moreover, the speedup achieved by *Élivágar* increases with benchmark size despite the reduced cost of gradient computation, highlighting *Élivágar*'s resource-efficiency.

Table 4: Absolute runtimes (in minutes) for *Élivágar* and QuantumNAS for different benchmarks when using *classical simulators*, and speedups experienced by *Élivágar* when running on *classical simulators* (C) and *real quantum hardware* (Q).

Benchmark	QNAS	<i>Élivágar</i>	Speedup (C)	Speedup (Q)
Moons	43.4	7.7	5.6x	44x
Vowel-4	63.3	8.9	7.0x	77x
Vowel-2	58.6	9.4	6.2x	104x
Bank	48.9	7.6	6.4x	119x
MNIST-2	143.6	7.8	18.6x	182x
FMNIST-2	184.3	8.3	22.0x	282x
FMNIST-4	228.6	11.1	20.7x	646x
MNIST-4	174.2	15.4	11.3x	1046x
MNIST-10	1007.8	35.5	28.4x	5220x
GMean			11.7x	271x

8.2.2. Using quantum hardware

In this scenario, all training is done via the parameter-shift rule [87], which results in drastically increased training costs, as explained in Section 2. Unfortunately, the high variance in the times required to run circuits on quantum hardware via a cloud computing platform make it near impossible to reliably estimate runtimes via wall-clock time. Consequently, the most reliable way to estimate the speedup achieved by *Élivágar* is to compare the number of circuit executions required by both methods for each benchmark. Table 4 shows the speedups achieved by *Élivágar*, which is 271 \times times faster than QuantumNAS on average. We provide a detailed breakdown of this speedup in Section 9.4.

Table 5: Characteristics of Élivágar-generated (no optimization) and device-unaware random circuits (SABRE [35] + Qiskit compiler level 3) run on *real quantum hardware*. Fidelity refers to the extent to which circuit outputs remain unaffected by noise, and is different from circuit accuracy (see Section 7.6).

Policy	2Q gates	2Q gates after compilation ↓	Fidelity ↑
OQC Lucy			
SABRE	7.04	16.22	0.595
Élivágar	7.04	7.04	0.706
IBM-Geneva			
SABRE	6.48	15.24	0.615
Élivágar	6.48	6.48	0.714
IBMQ-Kolkata			
SABRE	9.52	22.16	0.741
Élivágar	9.52	9.52	0.848
IBMQ-Mumbai			
SABRE	9.75	25.00	0.634
Élivágar	9.75	9.75	0.804

9. Performance Analysis

9.1. Device-aware circuit generation

To analyze Élivágar’s circuit generation strategy, we compare device-aware circuits generated via Algorithm 1 with randomly generated, device-unaware circuits. We generate pairs of device-aware and -unaware circuits with the same number of 1- and 2-qubit gates before compilation to ensure a fair comparison. Device-aware circuits are run unoptimized, but device-unaware circuits are optimized using level 3 of the Qiskit compiler and SABRE [35]. Table 5 shows that device-aware circuits have 18.9% higher fidelity on average. Thus, Élivágar’s circuit generation strategy not only eliminates the need for a circuit-mapping co-search, but also boosts circuit noise robustness, reducing performance degradation.

9.2. Circuit statistics

The statistics for the compiled and optimized circuits used for the Bank and Vowel-2 benchmarks are shown in Table 6. Random and Human Design are noise and device unaware, resulting in large, deep circuits (depths 163, 260 for MNIST-4, and 211, 344 for MNIST-10) with many two-qubit gates even after optimization using level 3 of the Qiskit compiler. As a result, these circuits experience a large reduction in accuracy when run on real devices compared to their noise-free performance. QuantumSupernet is noise and device-aware, but uses a deep embedding subcircuit that requires multiple layers of

Table 6: Compiled circuit statistics for Élivágar and competing methods run on *real quantum hardware*.

Method	1Q Gates ↓	2Q Gates ↓	Depth ↓	Acc. ↑
Vowel-2 (32 params.) on IBM Nairobi				
Random	171	52	139	0.653
Human Designed	194	52	139	0.508
QuantumSupernet	118	51	104	0.533
QuantumNAS	67	9	37	0.716
Élivágar	61	7	30	0.825
MNIST-4 (40 params.) on IBM Lagos				
Random	201	60	163	0.552
Human Designed	252	155	260	0.550
QuantumSupernet	218	122	206	0.300
QuantumNAS	61	5	32	0.625
Élivágar	45	4	20	0.642
MNIST-10 (72 params.) on IBM Osaka				
Random	89	87	211	0.128
Human Designed	355	228	344	0.113
QuantumNAS	121	22	55	0.190
Élivágar	107	24	49	0.178

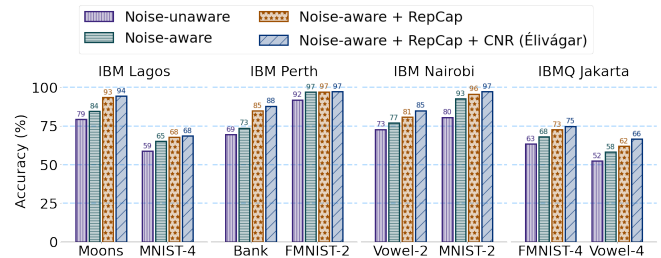


Figure 9: Each component of Élivágar - device- and noise-aware circuit generation, RepCap, and CNR - contributes to the final accuracy of the selected circuit. All values are absolute classification accuracies obtained on *noisy simulators*. Each bar shows the mean of 25 runs.

entangling CRY gates, and thus undergoes significant accuracy reduction as well. The circuits found by QuantumNAS and Élivágar are much shallower due to the evolutionary search and CNR incentivizing the selection of shallow, noise-robust circuits, respectively.

However, despite being similarly noise-robust and shallow, the circuits found by Élivágar perform significantly better than those found by QuantumNAS, likely due to the difference in the embeddings used by the circuits. We explore the effect of searching for data embeddings in detail in Section 9.3.

9.3. Breakdown of performance improvement

We break down *Élivágar*'s performance improvement into three parts: device-aware circuit generation (Section 4), RepCap and data embeddings (Section 6), and CNR (Section 5) in Fig. 9. We use 8 benchmarks from Table 2, and compare *Élivágar* to three baselines: (1) device- and noise-unaware circuits, (2) hardware-efficient device- and noise-aware random circuits generated via Algorithm 1, and (3) circuits found by *Élivágar* using only RepCap, i.e. without using CNR to rank circuits.

Using device- and noise-aware circuits increases accuracy over device-unaware circuits by 5%, further demonstrating the improved noise-robustness of circuits generated using Algorithm 1. The biggest accuracy improvement (6%) is obtained by using RepCap to select circuits instead of choosing randomly, highlighting the importance of strong predictors of circuit performance.

Using RepCap to select circuits allows *Élivágar* to search for both data embeddings and variational gates. To isolate the effect of searching for data embeddings, we compare *Élivágar* with versions of *Élivágar* that use fixed angle [7] and IQP embeddings [24]. We evaluate the three versions of *Élivágar* using a noiseless simulator to eliminate the effects of noise. As shown in Fig. 10, *Élivágar* obtains 5.5% and 20% higher accuracy when searching for data embeddings than when using a fixed angle and IQP embedding, respectively. This is because searching for embeddings allows *Élivágar* to co-search for suitable combinations of embeddings and variational gates, allowing it to find higher performance circuits than when using a fixed embedding. Thus, almost all of the accuracy gains achieved by using RepCap is due to the data embedding search, reinforcing the significance of data embeddings in determining performance on QML tasks.

Finally, using CNR in addition to RepCap further increases accuracy by 2% on average. Using both predictors results in better performance than only using RepCap as while using RepCap leads to *Élivágar* choosing circuits with high noiseless accuracy, RepCap is not device- and noise-aware and thus may choose circuits that are not noise-robust, leading to large accuracy degradations when run on real hardware. Using both predictors allows *Élivágar* to balance circuit learning capability and expressivity with circuit noise robustness to find a circuit that can accurately learn the target dataset while also being robust to hardware noise.

9.4. Breakdown of runtime speedup

When training on quantum hardware, the speedup of *Élivágar* over QuantumNAS comes from (1) using representational capacity for performance evaluation, (2) early rejection of low-fidelity circuits, and (3) eliminating the circuit-mapping co-search by generating device-aware circuits. Using representational capacity speeds up *Élivágar* by $16\times$ – $78\times$ for the benchmarks in Section 8, growing with problem size. Since

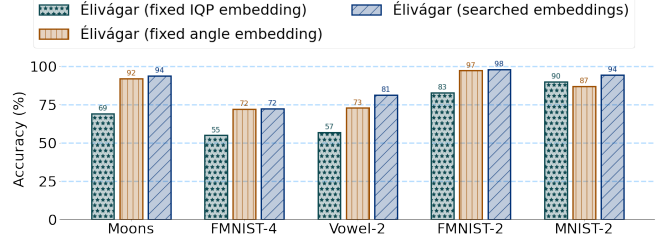


Figure 10: Performance of *Élivágar* when searching for data embeddings versus when using a fixed data embedding. All values are absolute classification accuracies obtained on *noiseless simulators*. Each bar shows the mean of 25 runs.

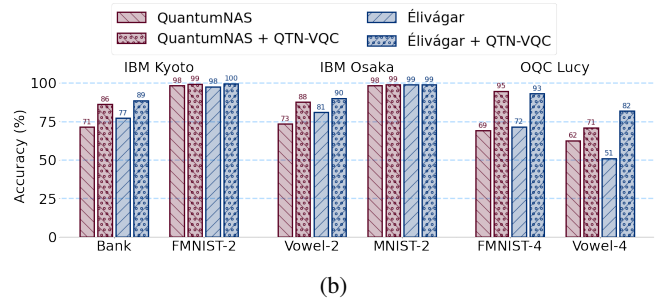
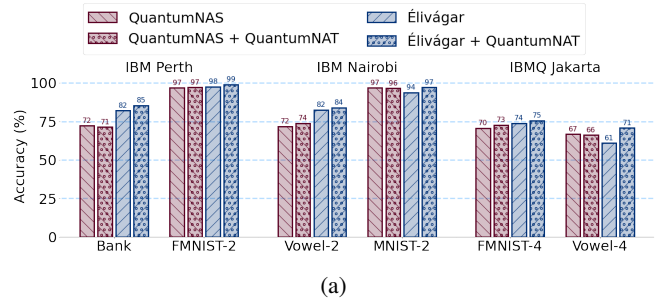


Figure 11: Results on *real quantum hardware* when performing training and inference with and without (a) QuantumNAT [82] and (b) QTN-VQC [66]. All values are absolute classification accuracies.

we use conservative CNR hyperparameter values, the speedup due to early rejection for all tasks is $2\times$. Eliminating the circuit-mapping co-search provides a speedup of $1.4\times$ – $33.4\times$, growing with problem size.

9.5. Compatibility with other QML frameworks

Élivágar is compatible with frameworks targeting the data preprocessing and training stages of the QML pipeline, such as QTN-VQC [66] and QuantumNAT [82], and makes no assumptions about how these tasks are performed. These frameworks can be combined with *Élivágar* to further boost circuit performance. Fig. 11a compares the performance of *Élivágar* and QuantumNAS with and without QuantumNAT [82], a framework that aims to increase the noise robustness of circuits during training and inference. *Élivágar* obtains 2.2% higher accuracy than QuantumNAS + QuantumNAT, and 5.5% higher accuracy when paired with QuantumNAT.

We further combine Élivágar and QuantumNAS with QTN-VQC, a framework that performs classical preprocessing of input data via a trainable tensor network, with results shown in Fig. 11b. Even when using QTN-VQC, which significantly boosts performance due to the added classical trainable parameters in the tensor network used for preprocessing, Élivágar outperforms QuantumNAS by 2.4% on average.

10. Related works

10.1. Quantum Machine Learning

Several theoretical works have illustrated potential quantum advantage in tasks such as classification [1, 28] and regression [62]. Various approaches to QML have been proposed, including using quantum circuits as kernel methods [9, 21, 23, 24, 28, 33, 41, 72, 85], and as quantum neural networks [5, 20, 34, 51, 57, 66, 75, 76, 81, 97]. Multiple works [1, 76] introduced metrics that estimate circuit performance, but they are unsuitable for QCS due to their high cost.

10.2. Noise-aware quantum compilation and training

Recent compilation works explore different circuit transformations to improve noise robustness, including gate cancellation [31, 49, 90], qubit mapping and routing [3, 39, 40, 44, 47, 50, 55, 56, 77, 79, 88], error mitigation [13, 16, 58, 59], circuit synthesis [60, 61, 63, 86, 93], and pulse-level optimizations [22, 37, 46, 74]. Some of these works [13, 14, 67] use Clifford replicas to characterize device noise or create enhanced compilation passes. Élivágar, in contrast, applies Clifford replicas to QML, and uses them to perform a noise-guided search for QML circuits. Other works [82, 83] focus on increasing noise robustness for QML circuits through improved training procedures, an approach complementary to Élivágar, as these techniques can be combined with Élivágar to improve the training of circuits selected by Élivágar.

10.3. QCS for Variational Quantum Algorithms (VQAs)

A few studies have explored QCS for VQAs [11], such as QAOA [91], VQE [30], and state preparation [25, 92, 94]. These works largely adopt techniques from classical NAS. For example, QCEAT [30] is similar to evolutionary search-based NAS [69], and MCTS-QAOA [91] uses a reinforcement learning-based search algorithm inspired by [2, 95]. These frameworks can be extended to perform QCS for QML tasks, despite being originally designed for VQAs. However, since they rely on classically-inspired search and candidate evaluation mechanisms, these methods face the same issues as QCS works for QML, and are extremely slow even for small QML tasks. We compare Élivágar with [30, 91] in Table 1.

10.4. Data embeddings

Several works [10, 62, 73] have theoretically investigated the effect of data embeddings on circuit performance through the lens of generalization bounds and Fourier series. These works

focus on developing theory that relates the data embeddings used to trained circuit performance. As such, they use simplified settings that do not account for hardware noise or limited device connectivity, and place strict constraints of the structures of the circuits used. Thus, they cannot be used as tools for QCS directly. In contrast, Élivágar solves the near-term problem of identifying performant circuits for QML applications on NISQ hardware, which is a fundamentally different task. Élivágar, however, applies these theoretical insights on data embeddings to QCS by searching for both optimal data embeddings and variational gates for a QML task, which allows Élivágar to outperform prior QCS works.

10.5. QCS for QML

A few studies have focused on QCS for QML tasks, such as QuantumNAS [80] and QuantumSupernet [18]. These methods are both based on the classical Supernet [64] framework, and have been extensively discussed in Section 1, and compared with Élivágar in Section 8. Élivágar eschews the SuperCircuit that [18, 80] use in favor of a novel QCS pipeline that leverages training- and gradient-free circuit performance and noise robustness predictors to avoid expensive gradient computation. Thus, Élivágar avoids the runtime bottlenecks of SuperCircuit-based QCS frameworks, and is able to perform QCS with low overheads. In Table 1, we present a summary of the differences between Élivágar and prior works.

11. Conclusion

In this work, we present Élivágar, a noise-guided, resource-efficient QCS framework that searches for high-performance variational quantum circuits for QML tasks. Élivágar proposes that QCS methods should be tailored to QML tasks and carefully consider realistic constraints of QML algorithms and NISQ quantum hardware. Based on this proposal, Élivágar addresses the issues in current classically-inspired QCS methods and innovates in all important aspects of QCS with its topology-aware and data embedding-aware search space, noise-guided search algorithm, and two-stage circuit evaluation strategy. Comprehensive experimental results show that Élivágar significantly outperforms leading QCS methods while achieving much more favorable resource efficiency and scalability. Due to its resource efficiency and improved search space, Élivágar provides a powerful tool for enabling new research in QML and noise-aware quantum compilation.

Acknowledgements

S.A. thanks Sidharth Ramanan for fruitful discussions and comments on various drafts. Y.S. thanks Gushu Li for helpful reviews on the paper draft. We thank Prof. Devsh Tiwari for shepherding the paper and for providing detailed feedback. This work was funded in part by EPiQC, an NSF Expedition in Computing, under grant CCF-173044.

References

- [1] Amira Abbas, David Sutter, Christa Zoufal, Aurelien Lucchi, Alessio Figalli, and Stefan Woerner. The power of quantum neural networks. *Nature Computational Science*, 1(6):403–409, Jun 2021.
- [2] Bowen Baker, Otkrist Gupta, Nikhil Naik, and Ramesh Raskar. Designing neural network architectures using reinforcement learning. In *5th International Conference on Learning Representations, ICLR 2017, Toulon, France, April 24-26, 2017, Conference Track Proceedings*, 2017.
- [3] Jonathan M Baker, Casey Duckering, Alexander Hoover, and Frederic T Chong. Time-sliced quantum circuit partitioning for modular architectures. In *Computing Frontiers*, pages 98–107, 2020.
- [4] Atilim Gunes Baydin, Barak A. Pearlmutter, Alexey Andreyevich Radul, and Jeffrey Mark Siskind. Automatic differentiation in machine learning: a survey. *Journal of Machine Learning Research*, 18(153):1–43, 2018.
- [5] Marcello Benedetti, Erika Lloyd, Stefan Sack, and Mattia Fiorentini. Parameterized quantum circuits as machine learning models. *Quantum Science and Technology*, 4(4):043001, Nov 2019.
- [6] Ville Bergholm, Josh Izaac, Maria Schuld, Christian Gogolin, M Sohaib Alam, Shah Nawaz Ahmed, Juan Miguel Arrazola, Carsten Blank, Alain Delgado, Soran Jahangiri, et al. Pennylane: Automatic differentiation of hybrid quantum-classical computations. *arXiv preprint arXiv:1811.04968*, 2018.
- [7] Jacob Biamonte, Peter Wittek, Nicola Pancotti, Patrick Rebentrost, Nathan Wiebe, and Seth Lloyd. Quantum machine learning. *Nature*, 549(7671):195–202, 2017.
- [8] Sergey Bravyi and David Gosset. Improved classical simulation of quantum circuits dominated by clifford gates. *Phys. Rev. Lett.*, 116:250501, Jun 2016.
- [9] Abdulkadir Canatar, Evan Peters, Cengiz Pehlevan, Stefan M. Wild, and Ruslan Shaydulin. Bandwidth enables generalization in quantum kernel models. *Transactions on Machine Learning Research*, 2023.
- [10] Matthias C. Caro, Elies Gil-Fuster, Johannes Jakob Meyer, Jens Eisert, and Ryan Sweke. Encoding-dependent generalization bounds for parametrized quantum circuits. *Quantum*, 5:582, nov 2021.
- [11] M. Cerezo, Andrew Arrasmith, Ryan Babbush, Simon C. Benjamin, Suguru Endo, Keisuke Fujii, Jarrod R. McClean, Kosuke Mitarai, Xiao Yuan, Lukasz Cincio, and Patrick J. Coles. Variational quantum algorithms. *Nature Reviews Physics*, 3(9):625–644, 2021.
- [12] M. Cerezo, Akira Sone, Tyler Volkoff, Lukasz Cincio, and Patrick J. Coles. Cost function dependent barren plateaus in shallow parametrized quantum circuits. *Nature Communications*, 12(1), mar 2021.
- [13] Poulami Das, Siddharth Dangwal, Swamit S Tannu, and Moinuddin Qureshi. ADAPT: Mitigating idling errors in qubits via adaptive dynamical decoupling. In *MICRO*, 2021.
- [14] Poulami Das, Eric Kessler, and Yunong Shi. The imitation game: Leveraging copycats for robust native gate selection in nisq programs. In *HPCA 2023*, 2022.
- [15] Poulami Das, Swamit Tannu, Siddharth Dangwal, and Moinuddin Qureshi. ADAPT: Mitigating idling errors in qubits via adaptive dynamical decoupling. In *MICRO-54: 54th Annual IEEE/ACM International Symposium on Microarchitecture*. ACM, oct 2021.
- [16] Poulami Das, Swamit S Tannu, and Moinuddin Qureshi. Jigsaw:boosting fidelity of nisq programs via measurement subsetting. In *MICRO*, 2021.
- [17] Xuanyi Dong and Yi Yang. Searching for a robust neural architecture in four gpu hours. In *Proceedings of the IEEE Conference on Computer Vision and Pattern Recognition (CVPR)*, pages 1761–1770, 2019.
- [18] Yuxuan Du, Tao Huang, Shan You, Min-Hsiu Hsieh, and Dacheng Tao. Quantum circuit architecture search for variational quantum algorithms. *npj Quantum Information*, 8(1):62, May 2022.
- [19] Andreas Elben, Steven T. Flammia, Hsin-Yuan Huang, Richard Kueng, John Preskill, Benoît Vermersch, and Peter Zoller. The randomized measurement toolbox. *Nature Reviews Physics*, 5(1):9–24, Jan 2023.
- [20] Edward Farhi and Hartmut Neven. Classification with quantum neural networks on near term processors. *arXiv preprint arXiv:1802.06002*, 2018.
- [21] Jennifer R. Glick, Tanvi P. Gujarati, Antonio D. Corcoles, Youngseok Kim, Abhinav Kandala, Jay M. Gambetta, and Kristan Temme. Covariant quantum kernels for data with group structure. *Bulletin of the American Physical Society*, 2022.
- [22] Pranav Gokhale, Ali Javadi-Abhari, Nathan Earnest, Yunong Shi, and Frederic T Chong. Optimized quantum compilation for near-term algorithms with openpulse. In *MICRO*, pages 186–200. IEEE, 2020.
- [23] Tobias Haug, Chris N Self, and M S Kim. Quantum machine learning of large datasets using randomized measurements. *Machine Learning: Science and Technology*, 4(1):015005, jan 2023.
- [24] Vojtěch Havlíček, Antonio D. Córcoles, Kristan Temme, Aram W. Harrow, Abhinav Kandala, Jerry M. Chow, and Jay M. Gambetta. Supervised learning with quantum-enhanced feature spaces. *Nature*, 567(7747):209–212, mar 2019.
- [25] Zhimin He, Chuangtao Chen, Lvzhou Li, Shenggen Zheng, and Haozhen Situ. Quantum architecture search with meta-learning. *Advanced Quantum Technologies*, 5(8):2100134, 2022.
- [26] He-Liang Huang, Yuxuan Du, Ming Gong, Youwei Zhao, Yulin Wu, Chaoyue Wang, Shaowei Li, Futian Liang, Jin Lin, Yu Xu, Rui Yang, Tongliang Liu, Min-Hsiu Hsieh, Hui Deng, Hao Rong, Cheng-Zhi Peng, Chao-Yang Lu, Yu-Ao Chen, Dacheng Tao, Xiaobo Zhu, and Jian-Wei Pan. Experimental quantum generative adversarial networks for image generation. *Physical Review Applied*, 16(2), aug 2021.
- [27] Hsin-Yuan Huang, Michael Broughton, Jordan Cotler, Sitan Chen, Jerry Li, Masoud Mohseni, Hartmut Neven, Ryan Babbush, Richard Kueng, John Preskill, and Jarrod R. McClean. Quantum advantage in learning from experiments. *Science*, 376(6598):1182–1186, jun 2022.
- [28] Hsin-Yuan Huang, Michael Broughton, Masoud Mohseni, Ryan Babbush, Sergio Boixo, Hartmut Neven, and Jarrod R. McClean. Power of data in quantum machine learning. *Nature Comms.*, 12(1):2631, 2021.
- [29] Hsin-Yuan Huang, Richard Kueng, and John Preskill. Predicting many properties of a quantum system from very few measurements. *Nature Physics*, 16(10):1050–1057, jun 2020.
- [30] Yuhang Huang, Qingyu Li, Xiaokai Hou, Rebing Wu, Man-Hong Yung, Abolfazl Bayat, and Xiaoting Wang. Robust resource-efficient quantum variational ansatz through an evolutionary algorithm. *Physical Review A*, 105(5), may 2022.
- [31] Raban Iten, Romain Moyard, Tony Metger, David Sutter, and Stefan Woerner. Exact and practical pattern matching for quantum circuit optimization. *ACM Transactions on Quantum Computing*, 3(1), jan 2022.
- [32] E. Knill, D. Leibfried, R. Reichle, J. Britton, R. B. Blakestad, J. D. Jost, C. Langer, R. Ozeri, S. Seidelin, and D. J. Wineland. Randomized benchmarking of quantum gates. *Physical Review A*, 77(1), jan 2008.
- [33] Jonas M. Kübler, Simon Buchholz, and Bernhard Schölkopf. The inductive bias of quantum kernels. In A. Beygelzimer, Y. Dauphin, P. Liang, and J. Wortman Vaughan, editors, *Advances in Neural Information Processing Systems*, 2021.
- [34] Martín Larocca, Nathan Ju, Diego García-Martín, Patrick J. Coles, and Marco Cerezo. Theory of overparametrization in quantum neural networks. *Nature Computational Science*, 3(6):542–551, Jun 2023.
- [35] Gushu Li, Yufei Ding, and Yuan Xie. Tackling the qubit mapping problem for nisq-era quantum devices. In *Proceedings of the Twenty-Fourth International Conference on Architectural Support for Programming Languages and Operating Systems, ASPLOS ’19*, page 1001–1014, New York, NY, USA, 2019. Association for Computing Machinery.
- [36] Liam Li and Ameet Talwalkar. Random search and reproducibility for neural architecture search. In Ryan P. Adams and Vibhav Gogate, editors, *Proceedings of The 35th Uncertainty in Artificial Intelligence Conference*, volume 115 of *Proceedings of Machine Learning Research*, pages 367–377. PMLR, 22–25 Jul 2020.
- [37] Zhiding Liang, Jinglei Cheng, Hang Ren, Hanrui Wang, Fei Hua, Yongshan Ding, Fred Chong, Song Han, Yiyu Shi, and Xuehai Qian. Pan: Pulse ansatz on nisq machines. *arXiv preprint arXiv:2208.01215*, 2022.
- [38] Hanxiao Liu, Karen Simonyan, and Yiming Yang. DARTS: Differentiable architecture search. In *International Conference on Learning Representations*, 2019.
- [39] Ji Liu, Luciano Bello, and Huiyang Zhou. Relaxed peephole optimization: A novel compiler optimization for quantum circuits. In *2021 IEEE/ACM International Symposium on Code Generation and Optimization (CGO)*, pages 301–314. IEEE, 2021.
- [40] Ji Liu, Peiyi Li, and Huiyang Zhou. Not all swaps have the same cost: A case for optimization-aware qubit routing. In *2022 IEEE International Symposium on High-Performance Computer Architecture (HPCA)*, pages 709–725. IEEE, 2022.
- [41] Yunchao Liu, Srinivasan Arunachalam, and Kristan Temme. A rigorous and robust quantum speed-up in supervised machine learning. *Nature Physics*, 17(9):1013–1017, jul 2021.
- [42] Seth Lloyd, Maria Schuld, Aroosa Ijaz, Josh Izaac, and Nathan Killoran. Quantum embeddings for machine learning. *arXiv preprint arXiv:2001.03622*, 2020.
- [43] Volker Lohweg. banknote authentication. UCI Machine Learning Repository, 2013. DOI: <https://doi.org/10.24432/C55P57>.

- [44] Aaron Lye, Robert Wille, and Rolf Drechsler. Determining the minimal number of swap gates for multi-dimensional nearest neighbor quantum circuits. In *ASPDAC*, pages 178–183. IEEE, 2015.
- [45] Jarrod R. McClean, Sergio Boixo, Vadim N. Smelyanskiy, Ryan Babbush, and Hartmut Neven. Barren plateaus in quantum neural network training landscapes. *Nature Communications*, 9(1), Nov 2018.
- [46] Dekel Meiron and Steven H. Frankel. Pansatz: Pulse-based ansatz for variational quantum algorithms. *arXiv preprint arXiv:2212.12911*, 2022.
- [47] Prakash Murali, Jonathan M Baker, Ali Javadi-Abhari, Frederic T Chong, and Margaret Martonosi. Noise-adaptive compiler mappings for noisy intermediate-scale quantum computers. In *ASPLOS*, 2019.
- [48] Prakash Murali, David C. McKay, Margaret Martonosi, and Ali Javadi-Abhari. Software mitigation of crosstalk on noisy intermediate-scale quantum computers. In *Proceedings of the Twenty-Fifth International Conference on Architectural Support for Programming Languages and Operating Systems*. ACM, mar 2020.
- [49] Yunseong Nam, Neil J. Ross, Yuan Su, Andrew M. Childs, and Dmitri Maslov. Automated optimization of large quantum circuits with continuous parameters. *npj Quantum Information*, 4(1):23, 2018.
- [50] Giacomo Nannicini, Lev S. Bishop, Oktay Günlük, and Petar Jurcevic. Optimal qubit assignment and routing via integer programming. *ACM Transactions on Quantum Computing*, 4(1), oct 2022.
- [51] Quynh T. Nguyen, Louis Schatzki, Paolo Braccia, Michael Ragone, Patrick J. Coles, Frederic Sauvage, Martin Larocca, and M. Cerezo. Theory for equivariant quantum neural networks. *arXiv preprint arXiv:2210.08566*, 2022.
- [52] Michael A. Nielsen and Isaac L. Chuang. *Quantum Computation and Quantum Information: 10th Anniversary Edition*. Cambridge University Press, New York, NY, USA, 10th edition, 2011.
- [53] Xuefei Ning, Changcheng Tang, Wenshuo Li, Zixuan Zhou, Shuang Liang, Huazhong Yang, and Yu Wang. Evaluating efficient performance estimators of neural architectures. In A. Beygelzimer, Y. Dauphin, P. Liang, and J. Wortman Vaughan, editors, *Advances in Neural Information Processing Systems*, 2021.
- [54] Murphy Yuezhen Niu, Alexander Zlokapa, Michael Broughton, Sergio Boixo, Masoud Mohseni, Vadim Smelyanskiy, and Hartmut Neven. Entangling quantum generative adversarial networks. *Phys. Rev. Lett.*, 128:220505, Jun 2022.
- [55] Angelo Oddi and Riccardo Rasconi. Greedy randomized search for scalable compilation of quantum circuits. In *International Conference on the Integration of Constraint Programming, Artificial Intelligence, and Operations Research*, pages 446–461. Springer, 2018.
- [56] Tirthak Patel, Daniel Silver, and Devesh Tiwari. Geysr: a compilation framework for quantum computing with neutral atoms. In *Proceedings of the 49th Annual International Symposium on Computer Architecture*, pages 383–395, 2022.
- [57] Tirthak Patel, Daniel Silver, and Devesh Tiwari. Optic: A practical quantum binary classifier for near-term quantum computers. In *Proceedings of the 2022 Conference and Exhibition on Design, Automation and Test in Europe*, DATE '22, page 334–339, Leuven, BEL, 2022. European Design and Automation Association.
- [58] Tirthak Patel and Devesh Tiwari. Disq: A novel quantum output state classification method on ibm quantum computers using openpulse. In *Proceedings of the 39th International Conference on Computer-Aided Design*, ICCAD '20, New York, NY, USA, 2020. Association for Computing Machinery.
- [59] Tirthak Patel and Devesh Tiwari. Qraft: reverse your quantum circuit and know the correct program output. In Tim Sherwood, Emery D. Berger, and Christos Kozyrakis, editors, *ASPLOS '21: 26th ACM International Conference on Architectural Support for Programming Languages and Operating Systems, Virtual Event, USA, April 19-23, 2021*, pages 443–455. ACM, 2021.
- [60] Tirthak Patel, Ed Younis, Costin Iancu, Wibe de Jong, and Devesh Tiwari. Quest: systematically approximating quantum circuits for higher output fidelity. In *Proceedings of the 27th ACM International Conference on Architectural Support for Programming Languages and Operating Systems*, pages 514–528, 2022.
- [61] Tirthak Patel, Ed Younis, Costin Iancu, Wibe de Jong, and Devesh Tiwari. Robust quantum circuit approximation for resource-efficient circuit synthesis. *Bulletin of the American Physical Society*, 2022.
- [62] Evan Peters and Maria Schuld. Generalization despite overfitting in quantum machine learning models. *arXiv preprint arXiv:2209.05523*, 2022.
- [63] Eric C Peterson, Lev S Bishop, and Ali Javadi-Abhari. Optimal synthesis into fixed xx interactions. *Quantum*, 6:696, 2022.
- [64] Hieu Pham, Melody Guan, Barret Zoph, Quoc Le, and Jeff Dean. Efficient neural architecture search via parameters sharing. In Jennifer Dy and Andreas Krause, editors, *Proceedings of the 35th International Conference on Machine Learning*, volume 80 of *Proceedings of Machine Learning Research*, pages 4095–4104. PMLR, 10–15 Jul 2018.
- [65] John Preskill. Quantum Computing in the NISQ era and beyond. *Quantum*, 2:79, August 2018.
- [66] Jun Qi, Chao-Han Huck Yang, and Pin-Yu Chen. Qtn-vqc: An end-to-end learning framework for quantum neural networks. *arXiv preprint arXiv:2110.03861*, 2021.
- [67] Gokul Subramanian Ravi, Jonathan M. Baker, Kaitlin N. Smith, Nathan Earnest, Ali Javadi-Abhari, and Frederic Chong. Boosting quantum fidelity with an ordered diverse ensemble of clifford canary circuits. *Bulletin of the American Physical Society*, 2022.
- [68] Gokul Subramanian Ravi, Pranav Gokhale, Yi Ding, William Kirby, Kaitlin Smith, Jonathan M. Baker, Peter J. Love, Henry Hoffmann, Kenneth R. Brown, and Frederic T. Chong. Cafqa: A classical simulation bootstrap for variational quantum algorithms. In *Proceedings of the 28th ACM International Conference on Architectural Support for Programming Languages and Operating Systems, Volume 1*, ASPLOS 2023, page 15–29, New York, NY, USA, 2022. Association for Computing Machinery.
- [69] Esteban Real, Alok Aggarwal, Yanping Huang, and Quoc V. Le. Regularized evolution for image classifier architecture search. In *Proceedings of the Thirty-Third AAAI Conference on Artificial Intelligence and Thirty-First Innovative Applications of Artificial Intelligence Conference and Ninth AAAI Symposium on Educational Advances in Artificial Intelligence*, AAAI'19/IAAI'19/EAAI'19. AAAI Press, 2019.
- [70] Manuel S. Rudolph, Ntwali Bashige Toussaint, Amara Katarbarwa, Sonika Johri, Borja Peropadre, and Alejandro Perdomo-Ortiz. Generation of high-resolution handwritten digits with an ion-trap quantum computer. *Phys. Rev. X*, 12:031010, Jul 2022.
- [71] Maria Schuld, Ville Bergholm, Christian Gogolin, Josh Izaac, and Nathan Killoran. Evaluating analytic gradients on quantum hardware. *Physical Review A*, 99(3), mar 2019.
- [72] Maria Schuld and Francesco Petruccione. *Quantum Models as Kernel Methods*, pages 217–245. Springer International Publishing, Cham, 2021.
- [73] Maria Schuld, Ryan Sweke, and Johannes Jakob Meyer. Effect of data encoding on the expressive power of variational quantum-machine-learning models. *Physical Review A*, 103(3), mar 2021.
- [74] Yunong Shi, Nelson Leung, Pranav Gokhale, Zane Rossi, David I Schuster, Henry Hoffmann, and Frederic T Chong. Optimized compilation of aggregated instructions for realistic quantum computers. In *ASPLOS*, 2019.
- [75] Daniel Silver, Tirthak Patel, and Devesh Tiwari. Quilt: Effective multi-class classification on quantum computers using an ensemble of diverse quantum classifiers. *Proceedings of the AAAI Conference on Artificial Intelligence*, 36(8):8324–8332, Jun. 2022.
- [76] Sukin Sim, Peter D. Johnson, and Alán Aspuru-Guzik. Expressibility and entangling capability of parameterized quantum circuits for hybrid quantum-classical algorithms. *Advanced Quantum Technologies*, 2(12):1900070, Oct 2019.
- [77] Kaitlin N Smith, Gokul Subramanian Ravi, Prakash Murali, Jonathan M Baker, Nathan Earnest, Ali Javadi-Abhari, and Frederic T Chong. Error mitigation in quantum computers through instruction scheduling. *arXiv preprint arXiv:2105.01760*, 2021.
- [78] Swamit Tannu, Poulami Das, Ramin Ayanzadeh, and Moinuddin Qureshi. HAMMER: boosting fidelity of noisy quantum circuits by exploiting hamming behavior of erroneous outcomes. In *Proceedings of the 27th ACM International Conference on Architectural Support for Programming Languages and Operating Systems*. ACM, feb 2022.
- [79] Swamit S Tannu and Moinuddin K Qureshi. Not all qubits are created equal: a case for variability-aware policies for nisq-era quantum computers. In *ASPLOS*, 2019.
- [80] H. Wang, Y. Ding, J. Gu, Y. Lin, D. Z. Pan, F. T. Chong, and S. Han. Quantumnas: Noise-adaptive search for robust quantum circuits. In *2022 IEEE International Symposium on High-Performance Computer Architecture (HPCA)*, pages 692–708, Los Alamitos, CA, USA, apr 2022. IEEE Computer Society.
- [81] Hanrui Wang, Jiaqi Gu, Yongshan Ding, Zirui Li, Frederic T. Chong, David Z. Pan, and Song Han. Roqnn: Noise-aware training for robust quantum neural networks. *arXiv preprint arXiv:2110.11331*, 2021.
- [82] Hanrui Wang, Jiaqi Gu, Yongshan Ding, Zirui Li, Frederic T. Chong, David Z. Pan, and Song Han. Quantumnat: Quantum noise-aware

- training with noise injection, quantization and normalization. In *Proceedings of the 59th ACM/IEEE Design Automation Conference, DAC '22*, page 1–6, New York, NY, USA, 2022. Association for Computing Machinery.
- [83] Hanrui Wang, Zirui Li, Jiaqi Gu, Yongshan Ding, David Z. Pan, and Song Han. Qoc: Quantum on-chip training with parameter shift and gradient pruning. In *Proceedings of the 59th ACM/IEEE Design Automation Conference, DAC '22*, page 655–660, New York, NY, USA, 2022. Association for Computing Machinery.
- [84] Samson Wang, Enrico Fontana, M. Cerezo, Kunal Sharma, Akira Sone, Lukasz Cincio, and Patrick J. Coles. Noise-induced barren plateaus in variational quantum algorithms. *Nature Communications*, 12(1):6961, Nov 2021.
- [85] Xinbiao Wang, Yuxuan Du, Yong Luo, and Dacheng Tao. Towards understanding the power of quantum kernels in the NISQ era. *Quantum*, 5:531, aug 2021.
- [86] Mathias Weiden, Justin Kalloor, Tirthak Patel, Ed Younis, Costin Iancu, and John Kubiawicz. Topology aware unitary synthesis for scalable quantum circuit optimization. *Bulletin of the American Physical Society*, 2022.
- [87] David Wierichs, Josh Izaac, Cody Wang, and Cedric Yen-Yu Lin. General parameter-shift rules for quantum gradients. *Quantum*, 6:677, mar 2022.
- [88] Robert Wille, Aaron Lye, and Rolf Drechsler. Optimal swap gate insertion for nearest neighbor quantum circuits. In *ASPDAC*. IEEE, 2014.
- [89] W. K. Wootters and W. H. Zurek. A single quantum cannot be cloned. *Nature*, 299(5886):802–803, 1982.
- [90] Mingkuan Xu, Zikun Li, Oded Padon, Sina Lin, Jessica Pointing, Auguste Hirth, Henry Ma, Jens Palsberg, Alex Aiken, Umut A Acar, et al. Quartz: superoptimization of quantum circuits. In *Proceedings of the 43rd ACM SIGPLAN International Conference on Programming Language Design and Implementation*, pages 625–640, 2022.
- [91] Jiahao Yao, Haoya Li, Marin Bukov, Lin Lin, and Lexing Ying. Monte carlo tree search based hybrid optimization of variational quantum circuits. In Bin Dong, Qianxiao Li, Lei Wang, and Zhi-Qin John Xu, editors, *Proceedings of Mathematical and Scientific Machine Learning*, volume 190 of *Proceedings of Machine Learning Research*, pages 49–64. PMLR, 15–17 Aug 2022.
- [92] Esther Ye and Samuel Yen-Chi Chen. Quantum architecture search via continual reinforcement learning. *arXiv preprint arXiv:2112.05779*, 2021.
- [93] Ed Younis, Koushik Sen, Katherine Yelick, and Costin Iancu. Qfast: Conflating search and numerical optimization for scalable quantum circuit synthesis. In *2021 IEEE International Conference on Quantum Computing and Engineering (QCE)*, pages 232–243. IEEE, 2021.
- [94] Shi-Xin Zhang, Chang-Yu Hsieh, Shengyu Zhang, and Hong Yao. Differentiable quantum architecture search. *Quantum Science and Technology*, 7(4):045023, aug 2022.
- [95] Barret Zoph and Quoc V. Le. Neural architecture search with reinforcement learning. In *5th International Conference on Learning Representations, ICLR 2017, Toulon, France, April 24-26, 2017, Conference Track Proceedings*, 2017.
- [96] Christa Zoufal. *Generative Quantum Machine Learning*. PhD thesis, ETH Zurich, 2021.
- [97] Christa Zoufal, Aurélien Lucchi, and Stefan Woerner. Variational quantum boltzmann machines. *Quantum Machine Intelligence*, 3(1), feb 2021.